The principal neurons of the medial nucleus of the trapezoid body and NG2$^+$ glial cells receive coordinated excitatory synaptic input

Jochen Müller,[1] Daniel Reyes-Haro,[1] Tatjyana Pivneva,[2] Christiane Nolte,[1] Roland Schaette,[3] Joachim Lübke,[4] and Helmut Kettenmann[1]

[1]Zelluläre Neurowissenschaften, Max-Delbrück-Centrum für Molekulare Medizin, 13092 Berlin, Germany
[2]Bogomoletz Institute of Physiology, 01024 Kiev, Ukraine
[3]Fachinstitut Theoretische Biologie, Humboldt-Universität zu Berlin, 10115 Berlin, Germany
[4]Institut für Neurowissenschaften und Biophysik, INB-3, 52425 Jülich, Germany

Glial cell processes are part of the synaptic structure and sense spillover of transmitter, while some glial cells can even receive direct synaptic input. Here, we report that a defined type of glial cell in the medial nucleus of the trapezoid body (MNTB) receives excitatory glutamatergic synaptic input from the calyx of Held (CoH). This giant glutamatergic terminal forms an axosomatic synapse with a single principal neuron located in the MNTB. The NG2 glia, as postsynaptic principal neurons, establish synapse-like structures with the CoH terminal. In contrast to the principal neurons, which are known to receive excitatory as well as inhibitory inputs, the NG2 glia receive mostly, if not exclusively, α-amino-3-hydroxy-5-methyl-isoxazole-4-propionic acid receptor–mediated evoked and spontaneous synaptic input. Simultaneous recordings from neurons and NG2 glia indicate that they partially receive synchronized spontaneous input. This shows that an NG2$^+$ glial cell and a postsynaptic neuron share presynaptic terminals.

The Journal of General Physiology

Downloaded from http://rupress.org/jgp/article-pdf/134/2/115/1787105/jgp_200910194.pdf by guest on 05 December 2025

INTRODUCTION

Glial cells have been shown to play an important role in synaptic behavior and are therefore part of the synaptic complex (Lin and Bergles, 2004b; Newman, 2005). The tight enwrapping of synapses by astrocytic processes restricts spillover of transmitter outside the synaptic cleft, thereby limiting intercellular crosstalk mediated by volume transmission (Oliet et al., 2004). The classical type of glial fibrillary acidic protein (GFAP)$^+$ astrocyte expresses glutamate transporters, and glutamatergic synaptic activity induces currents due to the glutamate uptake activity (Bergles and Jahr, 1997; Matthias et al., 2003). A second type of glial cell receives synaptic-like input from both glutamatergic and GABAergic terminals (Bergles et al., 2000; Matthias et al., 2003; Lin and Bergles, 2004a,b; Jabs et al., 2005; Lin et al., 2005; Kukley et al., 2007; Ziskin et al., 2007). The proteoglycan NG2 was reported to be a marker for this cell type. It has been termed oligodendrocyte precursor cell (Bergles et al., 2000), polydendrocyte, synantocyte (Butt et al., 2002), or receptor astrocyte (Matthias et al., 2003; Jabs et al., 2005). The Vitorio Gallo group was recently able to show coordinated input from CA3 pyramidal neurons onto NG2$^+$ glial cells and a subtype of GABAergic interneurons in the dentate gyrus (Mangin et al., 2008). However, it is still unknown whether synapses on this glial cell type are distinct contacts or if an NG2$^+$ cell and a neuron can receive common input from the same presynaptic terminal. In the present study, we investigated the interaction of NG2$^+$ glia with the giant glutamatergic nerve terminal, the so-called calyx of Held (CoH) (for review see von Gersdorff and Borst, 2002 and Schneggenburger and Forsythe, 2006). This synapse is part of the auditory pathway specialized for sound localization, which requires high-frequency signal transmission (McAlpine, 2005). This process involves neurons, the globular bushy cells of the anterior ventral cochlear nucleus that project via their axons to the principal neurons of the contralateral medial nucleus of the trapezoid body (MNTB) and form an axosomatic terminal, the CoH (Kuwabara et al., 1991). Presynaptic activation can be accomplished by electrical stimulation of the axons from the anterior ventral cochlear nucleus or by patch clamping a single CoH terminal (Barnes-Davies and Forsythe, 1995). The postsynaptic response is mediated by α-amino-3-hydroxy-5-methyl-isoxazole-4-propionic acid/kainic acid (AMPA/KA) and *N*-methyl-D-aspartate (NMDA) receptors (NMDARs) during the first 3 wk

J. Müller and D. Reyes-Haro contributed equally to this work.

Correspondence to Helmut Kettenmann: kettenmann@mdc-berlin.de

Abbreviations used in this paper: 4-AP, 4-aminopyridine; AMPA, α-amino-3-hydroxy-5-methyl-isoxazole-4-propionic acid; CoH, calyx of Held; D-Asp, D-aspartate; eGFP, enhanced green fluorescence protein; GFAP, glial fibrillary acidic protein; KA, kainic acid; LY, Lucifer yellow; MNTB, medial nucleus of the trapezoid body; NMDA, *N*-methyl-D-aspartate; NMDAR, NMDA receptor; sPSC, spontaneous postsynaptic current.

© 2009 Müller et al. This article is distributed under the terms of an Attribution–Noncommercial–Share Alike–No Mirror Sites license for the first six months after the publication date (see http://www.jgp.org/misc/terms.shtml). After six months it is available under a Creative Commons License (Attribution–Noncommercial–Share Alike 3.0 Unported license, as described at http://creativecommons.org/licenses/by-nc-sa/3.0/).

The Rockefeller University Press $30.00
J. Gen. Physiol. Vol. 134 No. 2 115–127
www.jgp.org/cgi/doi/10.1085/jgp.200910194

(Forsythe, 1994; Barnes-Davies and Forsythe, 1995; Joshi and Wang, 2002). Recent morphological studies revealed that glial processes contact the pre- and postsynaptic membranes of the CoH synapse and express both glutamate receptors and transporters (Elezgarai et al., 2001; Sätzler et al., 2002; Renden et al., 2005). However, none of these studies investigated a possible functional synaptic input onto glial cells, nor the concrete identity of the glial cells, namely astrocyte or NG2 glia, because expression of the glial marker GFAP has been observed in both cell types in several other brain regions. Thus, the aim of the present study was to characterize which types of glial cells are functionally associated with the CoH terminal and to study how they are involved in signal transduction at the CoH-principal neuron synapse in the MNTB.

MATERIALS AND METHODS

Preparation of brain stem slices

All experiments were performed according to the guidelines of the German animal protection law. For the experiments, 8–10-d-old out-bred NMRI mice (Charles River Laboratories) or transgenic GFAP–enhanced green fluorescence protein (eGFP) mice (Nolte et al., 2001) were used. For slice preparation, mice were decapitated and their brains were immediately transferred to ice-cold oxygenated artificial cerebrospinal fluid (aCSF) containing (in mM): 134 NaCl, 2.5 KCl, 1.3 $MgCl_2$, 2 $CaCl_2$, 1.25 K_2HPO_4, 26 $NaHCO_3$, and 10 glucose, equilibrated with 95% O_2 and 5% CO_2 to pH 7.4. Transverse brain stem slices (160–180 µm) were cut using a tissue slicer (Microm HM 650 V; Walldorf). The slices were gently transferred to a holding chamber and kept in CSF at room temperature for at least 45 min until they were used for recording.

Electrophysiological recordings

The MNTB was easily recognized using light microscopy due to the size of the principal neurons (~20 µm). Passive and complex glial cell and principal neuron somata in the MNTB were visible in standard water immersion optics and could be approached with a patch micropipette.

Membrane currents were recorded with the patch clamp technique in the whole cell recording configuration (Hamill et al., 1981). Current signals were amplified with a double EPC 9 (EPC9/2; HEKA), filtered at 3 kHz, sampled at 10 kHz, recorded by the TIDA software, and stored in a personal computer.

Patch micropipettes with a resistance of 3–5 MΩ (for the neurons) or 5–8 MΩ (for the glial cells) were pulled from thin-walled borosilicate glass (o.d., 1.5 mm; i.d., 0.87 mm; Hilgenberg) using a P2000 laser-based micropipette puller (Sutter Instrument Co.). The tip resistances resulted in uncompensated series resistances of 10–20 MΩ (for neurons) and 20–50 MΩ (for glial cells) at the beginning of the recordings. Recordings with series resistances higher than the above mentioned values were discarded from analysis. The micropipette solution used for neuronal recording in midline stimulation experiments and some experiments on spontaneous postsynaptic currents (sPSCs; as stated in the text) (solution A) contained (in mM): 97.5 potassium gluconate, 32.5 CsCl, 5 EGTA, 10 HEPES, 1 $MgCl_2$, 30 TEA, and 3 lidocaine *N*-ethyl bromide (QX314). For glial recording in midline stimulation experiments and some experiments on sPSCs (as mentioned in the text) (solution B), the internal solution contained (in mM): 120 potassium gluconate, 10 KCl, 1 $MgCl_2$, 10 HEPES, 0.1 EGTA, 0.025 $CaCl_2$, 1 K_2ATP, 4 glucose, and 0.2 Na_2 GTP. For all other experiments, we used an internal solution (solution C) containing (in mM): 130 KCl, 1 $MgCl_2$, 10 HEPES, 0.1 EGTA, 0.025 $CaCl_2$, 1 K_2ATP, 4 glucose, and 0.2 Na_2 GTP. The pH was adjusted to 7.2 with CsOH for solution A and KOH for solutions B and C.

All experiments were performed at room temperature (20–22°C). Chemicals were obtained from Sigma-Aldrich or Tocris if not otherwise indicated.

Slices were superfused with oxygenated artificial cerebrospinal fluid, and substances were applied by changing the perfusate. The analyses of the synaptic currents were performed with PeakCount software (Version 3.0.0) developed by Christian Henneberger at the Physiology Department of the Charité (Berlin, Germany), using a first-derivative threshold detection algorithm. The data were then used to compute the peak-to-peak time-difference histograms as well as the cross-correlation histograms.

Analysis of coincident events

For each event in the NG2 glia, we determined the temporally closest event in the neuron. The resulting time differences were used to construct the time-difference histogram with a temporal resolution (bin size) of 1 ms.

To calculate the probability of observing a certain number of coincident events by chance, events in the neuron and NG2 glia were treated as independent Poisson processes. When events occur at rate r_g in the NG2 glia and at rate r_n in the neuron, the probability p_c of observing both an event in NG2 glia and the neuron within a short time interval Δt is given by $p_c = r_n \Delta t\, r_g \Delta t$. The probability $p(n)$ of observing n coincident events (coincident defined as both events occurring within the same Δt) during a time period T that comprises $N = T/\Delta t$ short-time intervals is

$$p(n) = \binom{N}{n} p_c^n (1 - p_c)^{N-n} .$$

For the cross-correlation analysis, event trains were constructed from the event times in NG2 glia and neuron. Time was divided in 1-ms bins, and in each bin a 1 indicated the occurrence and a 0 the absence of an event. The resulting event trains (vectors) of NG2 glia and neuron were then cross-correlated using the MATLAB function xcorr, with time lags of −100 to +100 ms, yielding the raw count of coincident events for each time lag. A certain number n of coincident events was considered to be significant when

$$1 - \sum_{i=1}^{n} p(i) < \alpha,$$

i.e., when the probability of observing fewer coincident events exceeded $1 - \alpha$, with $\alpha = 0.05/z$ being the significance level with a Bonferroni correction for $z = 201$ tests (lags up to ± 100 ms in 1-ms steps in the cross-correlation analysis).

The analysis of coincident events was performed using MATLAB (The MathWorks Inc.).

Dye coupling experiments

During recording, cells were filled with Lucifer yellow (LY; 0.1%) and biocytin (0.5%) by dialyzing the cytoplasm with the patch pipette solution. To avoid destruction of the cell as the pipette was pulled off after recording, the seal was destroyed by a large hyperpolarizing current injection. After recording, LY fluorescence was examined in a two-photon laser scanning microscope, and then slices were fixed in 4% paraformaldehyde in 0.1 M phosphate buffer and stored there until biocytin detection. Biocytin

Downloaded from http://rupress.org/jgp/article-pdf/134/2/115/1787105/jgp_200910194.pdf by guest on 05 December 2025

detection was performed as described by D'Ambrosio et al. (1998) with few modifications, and sections were incubated with the Elite ABC kit (Vector Laboratories) for 48 h. The diaminobenzidine reaction was stopped after exactly 60 min; $NiCl_2$ was used for intensification. Slices were embedded in Aqua Poly/mount (Polysciences, Inc.). Images were taken with a digital camera (Axiocam; Carl Zeiss, Inc.) and appropriate software (Axiovision; Carl Zeiss, Inc.).

Immunohistochemistry

eGFP/GFAP transgenic mice (P8–P10) were deeply anesthetized with sodium pentobarbital (100 mg/kg body weight; Sanofi) and perfused intracardially with a solution of 4% paraformaldehyde in 0.1 M phosphate buffer (PB), pH 7.4. Brains were dissected out and postfixed for 2 h at 4°C. After several washes in PB, brains were incubated overnight in 30% sucrose in PB. The next day, they were quickly frozen in isopentane cooled by dry ice. 20-µm thick cryosections were mounted on gelatin-coated slides and allowed to dry for 30 min at room temperature. Sections were permeabilized with 0.1% Triton X-100 (TX100) in PB for 20 min and incubated in blocking solution (0.5% BSA, 4% normal goat serum [NGS], and 0.01% TX100 in PB) for 1 h at room temperature. Rabbit polyclonal antibodies to GFAP (Dako) were diluted 1:1,000 (in PB/1% BSA/1% NGS, 0.01% TX100). Sections were incubated with the primary antibodies for 24 h at 4°C. Primary antibodies were visualized by application of Alexa 568 goat anti–rabbit IgG (1:2,000; Invitrogen). Secondary antibodies were incubated for at least 2 h at room temperature. After three washes, sections were mounted with Aqua–Polymount (Polyscience Inc.) and inspected in the confocal microscope. Specificity of immunoreactivity was controlled by incubation of tissue sections in dilution buffer instead of primary antibodies. In the controls, the immunocytochemical reactions in the central nervous system were always negative. However, unspecific labeling of the meninges and connective tissue appeared in some cases.

Immunostaining for AN2 (NG2) of LY-filled cells

During recording, cells were filled with LY (0.1%) by dialyzing the cytoplasm with the patch pipette solution. To avoid destruction of the cell as the pipette was pulled off after recording, the seal was destroyed by a large hyperpolarizing current injection. Subsequently, slices were fixed for 30 min with 4% paraformaldehyde and then permeabilized with 0.5% TX100 in PBS, followed by treatment with PBS containing 0.5% TX100, 1% BSA, and 20% NGS. Slices were incubated overnight at 4°C with antibodies against AN2 (antibodies were provided by J. Trotter, Johannes Gutenberg University, Mainz, Germany). CY3-conjugated secondary antibodies were applied for 2 h at room temperature. Slices were shortly rinsed, mounted on slides as described above, and analyzed with a confocal laser scanning microscope equipped with a 488-nm argon ion laser (GE Healthcare) mounted on an upright microscope (Axioskop; Carl Zeiss, Inc.). eGFP fluorescence was excited at 457 nm (beam splitter, 510 nm) and detected with a 530-nm bandpass filter. Red fluorescence of Alexa or Cy3 was excited at 517 nm (beam splitter, 535 nm) and detected with a 570-nm long-pass filter. Confocal laser scanning microscope images were stored and processed on an Indigo workstation using the program Imagespace and superimposed by Adobe Photoshop.

Two-photon microscopy at the recording site

A two-photon laser scanning microscope (BX51WI; Olympus) with a 40× water-immersion objective lens was used to detect fluorescence signals (TILL Photonics). A Mira 900 laser (Coherent) tuned to 860 nm was used for excitation. Image acquisition was controlled by software (Fluoview FV300; Olympus). In the transfluorescence pathway, a 585-nm dichroic mirror was used to separate green and red fluorescence. D510/80M and HQ600LP filters were placed in the "green" and "red" pathways, respectively, to eliminate transmitted or reflected excitation light (Chroma Technology Corp.). For intracellular loading of cells, either LY (0.1%) or a combination of Alexa Fluor 568 (0.01%) and Alexa Fluor 594 (0.01%) was used to outline the cell structures.

Electron microscopy

Complex cells were identified by their current pattern and dialyzed via the patch electrode containing additional biocytin (0.5%) and LY (0.1%). Biocytin filling was judged to be complete when the LY fluorescence was visible in fine distal processes. Usually, the cells were completely stained after 15 min and the electrode was pulled off after the seal was damaged by a large hyperpolarizing current injection to avoid destruction of the cell membrane. Any extracellular biocytin deposits were readily washed out in PBS. Biocytin-stained slices were fixed with 4% paraformaldehyde and 1% glutaraldehyde for 3 h and rinsed with PBS for another 30 min. The tissue was incubated in 1.5 mg 3,3′-diaminobenzidine tetrahydrochloride (diaminobenzidine; Sigma-Aldrich) and 1 mg $NiCl_2$ per 1 ml PBS. The diaminobenzidine reaction was stopped while dark brown reaction became visible. The slices were then washed several times postfixed for 30 min in buffered 1% osmium tetroxide solution. They were dehydrated through graded concentrations of ethanol, pre-embedded with propylene oxide, and flat-embedded in epon. Ultrathin sections were stained with uranyl acetate and lead citrate and examined in an electron microscope (EM910; Carl Zeiss, Inc.) at 80 kV.

Statistical analysis

Statistical analyses were performed using Origin 7.0 software. The results are expressed as mean ± SD if not otherwise stated. When experiments included control and more than one test group, data were statistically evaluated with the Tukey test, a probe for ANOVA. We used Student's *t* test to compare two groups (control and test) within an experiment. p-values <0.05 were considered significant.

Online supplemental material

The online supplemental material contains images of dye coupling experiments (Fig. S1), bath application of KA on NG2 glia (Fig. S2), a cross correlation histogram of events in principal neuron and NG2 glia (Fig. S3), and bath application of NMDA and D-serine on NG2 glia (Fig. S4). The online supplemental material is available at http://www.jgp.org/cgi/content/full/jgp.200910194/DC1.

RESULTS

The CoH synapse is in contact with two types of glial cells

We identified two types of glial cells in close association with the CoH synapse that could be distinguished from each other by their eGFP fluorescence in GFAP-eGFP transgenic mice (Nolte et al., 2001). One type was highly fluorescent, with numerous ramified processes (Fig. 1 A, left). The second type was not or only weakly fluorescent (Fig. 1 A, left, arrow).

The identity of all recorded cells was routinely verified by applying a series of de- and hyperpolarizing voltage steps (Fig. 1 B). The cells with a high level of fluorescence had a resting membrane potential of −70 ± 3 mV, a membrane resistance of 27 ± 8 MΩ, and a membrane capacitance of 22.9 ± 16.4 pF (n = 25), whereas

Downloaded from http://rupress.org/jgp/article-pdf/134/2/115/1787105/jgp_200910194.pdf by guest on 05 December 2025

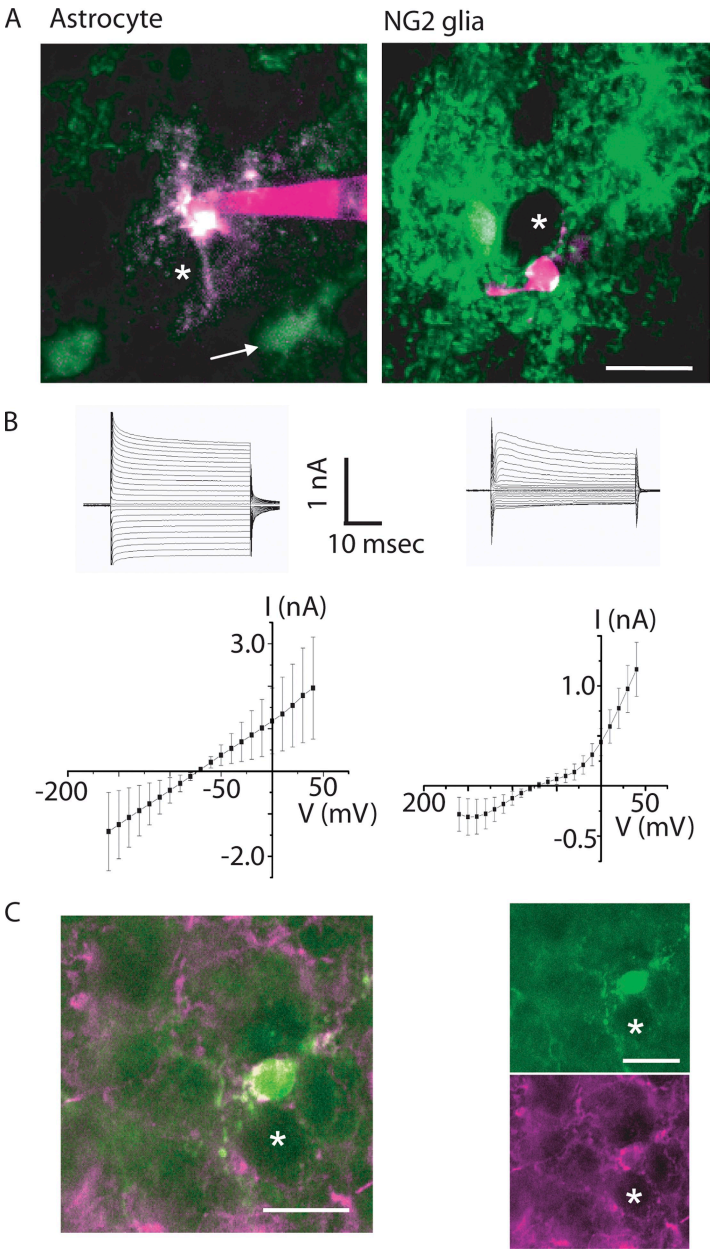

Figure 1. Identification of glial cells in the MNTB. (A) Astrocytes and NG2 glia in the MNTB of a GFAP-eGFP transgenic mouse. Images are overlays of five consecutive confocal sections taken 1-µm apart. The images are the overlays of eGFP (green) and Alexa 594 emission (magenta). Note that white color in the NG2 glia (right image) is not colocalization but is due to the z-stack projection. Asterisks indicate neighboring postsynaptic principal neurons. White arrow in the left image indicates weakly eGFP$^+$ glia. The scale bar (20 µm) refers to all pictures. (B) Electrophysiological identification of astrocyte and NG2 glia. (Top) Representative current responses from an astrocyte (left) and an NG2 glia (right) evoked by step voltages. Membrane currents were evoked by 50-ms voltage steps ranging from −160 to 40 mV from a holding potential of −70 mV. Scale bars refer to both graphs. (Bottom) Average current–voltage (IV) plots ($n = 25$). Data are mean ± SD. (C) MNTB glial cells with a complex current pattern and sPSCs are expressing AN2 antigen. Image on the left is an overlay of the two images on the right, showing a single focal plane of an NG2 glia filled with LY through the patch pipette (green), fixed after recording and proceeded for immunostaining with AN2 antibody (magenta; see Materials and methods). The asterisks indicate a neighboring principal neuron. The scale bar (20 µm) refers to all pictures.

the cells with low or no fluorescence had a membrane potential of −77 ± 8 mV, a membrane resistance of 159 ± 39 MΩ, and a low membrane capacitance (14.4 ± 5.4 pF; $n = 25$). The two cell types were also distinct in their membrane current pattern. The highly fluorescent cells showed passive membrane currents when de- and hyperpolarized between −160 to +40 mV for 50 ms resulting in a linear current–voltage relationship ($n = 25$; Fig. 1 B, left). In the low- or nonfluorescent cells, depolarizing voltage steps elicited currents with a delayed activation, sometimes preceded by small transient inward currents at potentials positive to −20 mV. With hyperpolarization only small currents were observed, resulting in an outward rectification of the current–voltage relationship ($n = 25$; Fig. 1 B, right). The peak currents at +40 mV were 1.96 ± 1.20 and 1.16 ± 0.27 nA for the fluorescent and nonfluorescent cells, respectively.

Fig. 1 A shows the morphologies of example recordings performed in brainstem slices of GFAP-eGFP mice. When Alexa 594 was injected via the patch pipette, a clear overlay of the eGFP and the Alexa signal was observed in cells with passive membrane currents, whereas no such overlay could be observed in cells with a complex current pattern. Therefore, the experiments were subsequently performed in NMRI wild-type mice and glial cells were visually identified and chosen for recording, due to the much smaller soma size compared with the principal neurons.

After recording membrane currents from cells from wild-type mice and dialyzing the cells with a solution

Downloaded from http://rupress.org/jgp/article-pdf/134/2/115/1787105/jgp_200910194.pdf by guest on 05 December 2025

containing LY, slices were fixed and labeled with an anti-AN2 antibody, the mouse homologue for the rat NG2 proteoglycan. All cells showing the complex current pattern were positive for AN2 ($n = 7$; Fig. 1 C).

Dye coupling experiments, where LY and biocytin were injected into glial cells, showed a network of coupled cells when the patched cell had a passive current profile ($n = 9$; Fig. S1). In contrast, dye coupling was never observed in cells with a complex current profile ($n = 32$; Fig. S1). Moreover, these cells responded to bath application of KA (0.5 mM) with an inward current (456 ± 132 pA; $n = 8$). Co-application of KA and the AMPA-KAR antagonist CNQX (50 µM) reduced the KA-induced current to 17% (27 ± 7 pA; $n = 7$; $P < 0.001$) (Fig. S2). On the other hand, D-aspartate (D-Asp; 0.5 mM), a substrate for glutamate transporters, did not elicited any response ($n = 6$; Fig. S2).

Collectively, these results identify the two glial cell types in the MNTB as the classical $GFAP^+$ astrocyte with high levels of GFAP expression and passive membrane currents, and $NG2^+$ glial cell with low or no GFAP expression and complex membrane currents. We will subsequently refer to these cells as astrocytes and NG2 glia, respectively.

NG2 glia form synapse-like contacts with the CoH

The morphology of NG2 glia was studied after biocytin injection and processing for subsequent electron microscopic analysis (Fig. 2). Consecutive ultrathin sections of biocytin-labeled NG2 glia ($n = 7$) were examined. Somata and fine processes of labeled NG2 glia were found in close proximity to the CoH terminal (Fig. 2, A and C). Processes of NG2 glia were frequently observed to contact both the presynaptic terminal and the postsynaptic principal neuron (Fig. 2, A and C). Presynaptic elements were sometimes ensheathed by fine glial processes (Fig. 2 B). In contrast to astrocytes (not depicted), synapse-like contact sites between processes of the NG2 glia and the CoH were detected (Fig. 2, B, D, and E). In addition, an accumulation of synaptic vesicles was frequently observed at the glial contact site. In some of the presynaptic structures, so-called docked vesicles were visible at the presynaptic densities (Fig. 2, D and E). A cleft-like structure containing electron-opaque material could also be detected. However, due to the strong labeling of NG2 glia by biocytin, it was not possible to identify a postsynaptic density. The length of synaptic-like junctions was 0.05–0.3 µm, but varied substantially from synapse to synapse as described for the cerebellar climbing fiber innervation of NG2-expressing glia (Lin et al., 2005). Collectively, our findings strongly imply that NG2 glia establish synapse-like contacts with the CoH. This type of synaptic contact was never observed between elements of NG2 glia and the post-synapse; i.e., principal neurons in the MNTB.

Stimulation of midline fibers triggers synaptic-like currents in NG2 glia

To test whether the synapse-like structures observed at the ultrastructural level have a functional correlate, we

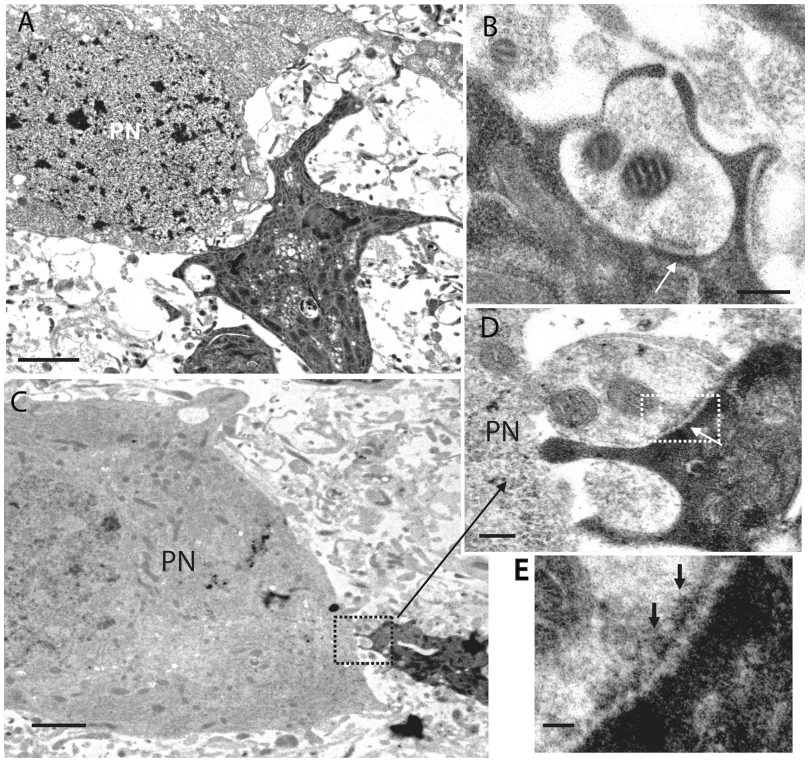

Figure 2. Ultrastructural evidence for synaptic junctions between CoH and NG2 glia. (A) Biocytin-labeled NG2 glia (dark profile) in close vicinity to a principal neuron (PN). (B) Example of a synaptic-like junction (arrow) between a finger of a CoH and a process of a biocytin-labeled NG2 glia as shown in A. (C) A labeled process of an NG2 glia is in contact with the CoH. (D) Higher magnification of the area delineated by the dashed rectangle in C shows a synaptic junction (arrow). Presynaptic areas contain small clear vesicles. (E) Consecutive section at higher magnification (the area in dashed rectangle in D; vesicles appear as docked to the presynaptic membrane [arrows]). Note a cleft-like structure that contains electron opaque material. (C–E) Obtained from the same NG2 glia. Bars: A and C, 2 µm; B and D, 0.2 µm; E, 0.1 µm.

Downloaded from http://rupress.org/jgp/article-pdf/134/2/115/1787105/jgp_200910194.pdf by guest on 05 December 2025

recorded membrane currents in NG2 glia and neighboring principal neurons during electrical stimulation of the midline fibers (1, 10, and 100 Hz; 0.1–1 mA). As described above, the cells were identified based on their current profile and morphology (Fig. 1, A and B). At 1 and 10 Hz, stimulation evoked inward currents that averaged 20.8 ± 4.0 pA in NG2 glia (range of 10.4 to 155.0 pA; n = 7; Fig. 3 A). The response of principal neurons was significantly larger when using the same stimulation protocol (2.2 ± 1.4 nA; range of 1.3 to 6.3 nA; P < 0.0001; Fig. 3 B). The decay time constant of the neuronal evoked postsynaptic currents (ePSCs) was 5.4 ± 4.5 ms (n = 5), therefore significantly slower than the one measured in NG2 glia (1.2 ± 1.0 ms; P < 0.001; n = 7). At 100 Hz, the current responses of NG2 glia showed a pronounced failure rate of 52 ± 22% (not depicted). This was in contrast to responses of principal neurons in the MNTB, which are known for their ability to cope with high stimulation frequencies up to several hundred Hz (Wu and Kelly, 1993).

Because the CoH synapse is glutamatergic and we were able to elicit membrane currents after bath application of 0.5 mM KA (Fig. S2), we applied 20 µM CNQX plus 50 µM APV, blockers of the AMPA-KAR and NMDAR, respectively. The current response of the NG2 glia was reversibly blocked (n = 7; Fig. 3, A and C). The response was also completely abolished when 1 µM TTX was added to the bath solution (n = 7; Fig. 3, A and C).

The responses were mainly mediated by AMPAR because 100 µM NMDA in combination with 10 µM D-serine did not induce any current response in four out of six cells and only a tiny current of <10 pA in two out of six cells (Fig. S4). We even assume that this small current was due to K^+ elevation–induced bei neuronal NMDAR activation.

sPSCs can be recorded in NG2 glia

sPSCs are rare at the principal neurons of the MNTB (Barnes-Davies and Forsythe, 1995), and the basal frequency was reported to be as low as 0.05 Hz (Kimura et al., 2003). In our preparation we observed a frequency of 0.16 ± 0.11 Hz (n = 20) in principal neurons (Fig. 4 A). In NG2 glia, we also observed spontaneous currents with a low frequency (0.11 ± 0.11 Hz; Fig. 4 A; n = 30). The spontaneous responses had a mean amplitude of 19 ± 12 pA in the neurons (n = 616 events in

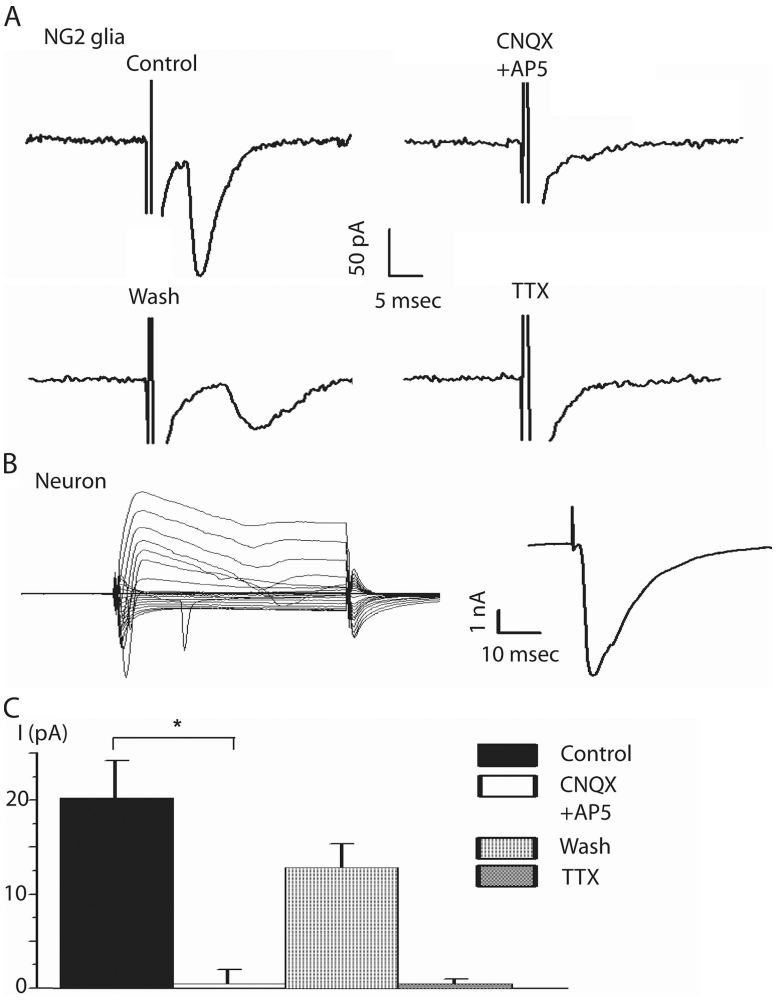

Figure 3. Evoked PSCs in NG2 glia and neurons. (A) Example traces showing responses of NG2 glia evoked by midline stimulation (stimulus intensity, 100 µA). (Top left row) Control conditions. (Top right row) The application of 20 µM CNQX and 50 µM AP5 to block AMPA-KAR and NMDAR, respectively. Reversibility inhibited the postsynaptic current. (Bottom left row) After 10 min of wash, the postsynaptic current partially recovered in the NG2 glia. (Bottom right row) 1 µM TTX abolished the current response. (B; Left) Current response from a principal neuron evoked by step voltages (50 ms; 10-mV increments) from −160 to +40 mV from a holding potential of −70 mV. (Right) Current response of the principal neuron shown on the left to midline stimulation with 100 µA (as applied to NG2 glia). (C) Summary of current responses to midline stimulation corresponding to the four experiments shown in A (n = 7). Data are the mean ± SEM. Asterisk represents significant difference (*, P = 0.02).

Downloaded from http://rupress.org/jgp/article-pdf/134/2/115/1787105/jgp_200910194.pdf by guest on 05 December 2025

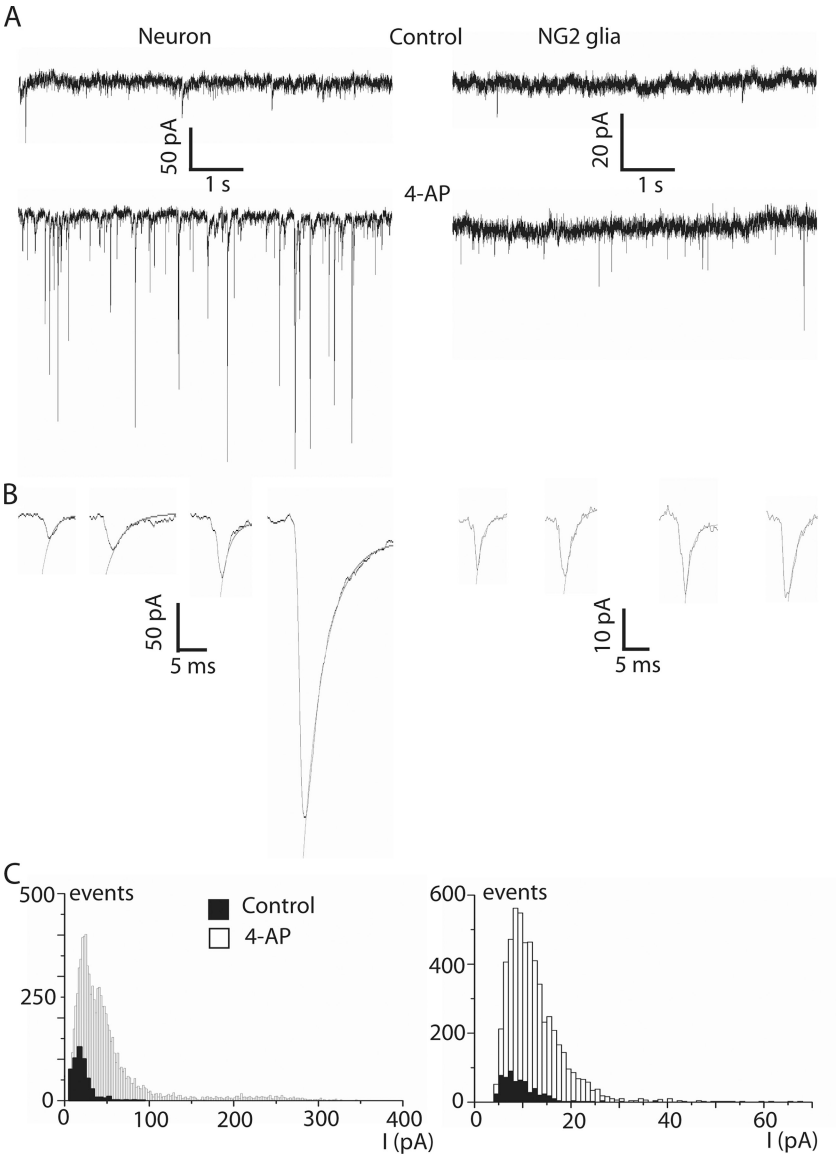

Figure 4. Spontaneous PSCs in NG2 glia and principal neurons of the MNTB. (A; Top row) sPSCs recorded simultaneously from a neuron and an NG2 glia under control conditions. (Bottom row) Bath application of 100 μM 4-AP increased the sPSC frequency in both cells. Note the amplitude difference in neuron and NG2 glia. (B) Single spontaneous events (shown with higher time resolution) fitted to a monoexponential. (C) Histograms of the amplitudes of sPSCs of 16 neurons and 26 NG2 glia recorded under control conditions (filled columns) or 4-AP (open columns).

20 cells) and 9.3 ± 4.4 pA in NG2 glia (n = 308 events in 28 cells; Fig. 4 C). The decay time constants of the sPSCs in neurons were 3.33 ± 1.60 ms (n = 616 events in 20 cells) and 1.85 ± 1.51 ms in NG2 glia ($P > 0.05$; n = 308 events in 28 cells). The 10–90% rise time of the neuronal events under these conditions was 0.58 ± 0.35 ms (n = 616 events in 20 cells), thus, significantly faster than the one obtained in the NG2 glia (0.72 ± 0.44 ms; $P = 0.003$; n = 308 events in 28 cells). Because the basal activity was very low, especially in NG2 glia, we performed our experiments under 4-aminopyridine (4-AP; 100 μM). This K^+ channel blocker enhances neurotransmitter release by depolarizing neurons and can be used to enhance spontaneous transmitter release (Flores-Hernandez et al., 1994). Indeed, application of 4-AP increased the frequency of spontaneous currents to 5.14 ± 4.96 Hz (n = 15; $P < 0.001$) in neurons and to 1.37 ± 2.21 Hz (n = 26) in NG2 glia ($P < 0.001$; Fig. 4, A and C). 4-AP also increased the mean amplitude of sPSCs to 53.4 ± 56.9 pA (n = 8,434 events in 15 cells; $P < 0.001$) in principal neurons and to 12.1 ± 6.1 pA (n = 2,756 events in 25 cells; $P < 0.001$) in NG2 glia (Fig. 4). The amplitude histograms of the spontaneous currents showed a peak at ∼20 pA for neurons and at ∼10 pA for NG2 glia (pooled data from 16 neurons and 26 NG2 glia; Fig. 4 C). From Fig. 4, it is evident that the majority of events in NG2 glia is within the amplitude range of ∼10 pA, whereas a significant number of events with higher amplitudes occurred in neurons.

The decay time constants of the sPSCs under 4-AP were 2.17 ± 2.48 (n = 2,756 events in 25 cells) and 4.70 ± 2.80 ($P > 0.05$; n = 8,434 events in 15 cells) in NG2 glia and neurons, respectively, thus not significantly different from the ones recorded under control conditions ($P > 0.05$).

Downloaded from http://rupress.org/jgp/article-pdf/134/2/115/1787105/jgp_200910194.pdf by guest on 05 December 2025

4-AP application increased the 10–90% rise time of the neuronal events to 1.01 ± 0.40 ms (n = 8,434 events in 15 cells), thus significantly different to the one observed under control conditions ($P < 0.001$). Rise times measured in the NG2 glia did not increase significantly after 4-AP application when compared with the control (0.86 ± 0.48 ms; $P > 0.05$; n = 2,756 events in 25 cells).

1 μM TTX almost completely abolished the spontaneous events stimulated by 4-AP in the NG2 glia (from 1.38 ± 1.10 to 0.01 ± 0.01 Hz; n = 5; P = 0.03).

To test for the impact of 4-AP on membrane currents in NG2 glia and postsynaptic neurons, the membrane was clamped with 50-ms voltage pulses from −160 to +70 mV in 10-mV steps. In NG2 glia, 100 μM 4-AP reduced the peak current at +70 mV by 32%, from 2.18 ± 0.57 nA to 1.48 ± 0.48 nA (n = 10; not depicted), and in neurons by 21%, from 2.57 ± 0.91 nA to 2.03 ± 0.81 nA (n = 11; not depicted).

sPSCs in NG2 glia are mediated by AMPA receptors

In principal neurons, 46% of the activity remained when CNQX was applied and the internal solution A (see Materials and methods) was used (n = 5), indicating that neurons receive additional inputs. Therefore, a cocktail of antagonists (2 μM strychnine, 10 μM gabazine, 50 μM D-APV, and 10 μM MK-801) was used in combination with internal solution B (see Materials and methods) to isolate AMPA-KAR–mediated currents and to compare them with those recorded in NG2 glia (Fig. 5). Under these conditions, the decay time of sPSCs in neurons was 3.0 ± 1.66 ms (n = 2,119 events), thus significantly different from the one obtained in the NG2 glia (1.88 ± 1.83 ms; $P < 0.05$; n = 237 events). The addition of CNQX to the cocktail almost abolished sPSCs in principal neurons; the sPSC rate dropped from 1.77 ± 1.40 to 0.06 ± 0.04 Hz (n = 6; $P < 0.001$).

To test for the receptor mediating the spontaneous postsynaptic events in the presence of 4-AP in NG2 glia,

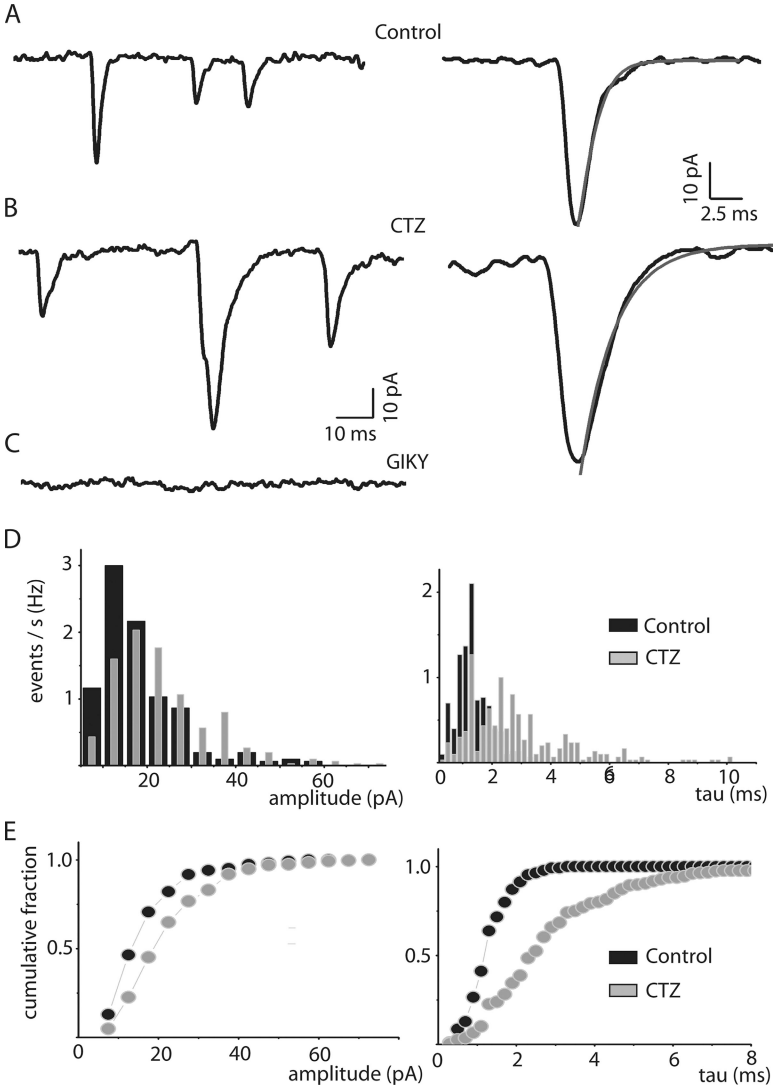

Figure 5. sPSCs recorded in NG2 glia are AMPA mediated. (A) sPSCs recorded during bath application of 100 μM 4-AP. A single event fitted to a monoexponential is shown with higher time resolution (right). (B) sPSCs recorded after preincubation with 100 μM CTZ and co-application of 100 μM 4-AP plus 100 μM CTZ. A single event, fitted to a monoexponential, is shown with higher time resolution (right). Note that the time decay constant (τ) under CTZ is slower than that observed with 4-AP alone. (C) 100 μM GYKI 52466 blocks the sPSCs completely. (D) Histograms of amplitude distribution (left) and time decay constants (right) under 4-AP and in the presence of CTZ. (E) Cumulative fraction for amplitude (left) and decay time constants (right).

Downloaded from http://rupress.org/jgp/article-pdf/134/2/115/1787105/jgp_200910194.pdf by guest on 05 December 2025

we applied the non-NMDAR antagonist CNQX (25 μM), the AMPA-specific antagonist GYKI 52466 (100 μM), or CTZ (100 μM), which blocks desensitization of AMPA receptors. CTZ did not influence the frequency of events (control 2.28 ± 3.92 Hz; $n = 5$, with CTZ 2.37 ± 4.15 Hz; $n = 4$; P = 0.94), but slowed the decay time constant from 1.34 ± 0.66 to 2.74 ± 1.8 (P < 0.001; Fig. 5, A and B). The addition of CNQX almost completely abolished the occurrence of sPSCs (0.09 ± 0.13 Hz; $n = 7$; P < 0.001; not depicted). Similarly, GYKI blocked sPSCs (0.03 ± 0.02 Hz; $n = 4$; Fig. 5 C; P < 0.001). This is also reflected in the decay time constant histogram (Fig. 5 D, right) and the cumulative fraction plot, which shows that the average decay time constant increases when CTZ is added (Fig. 5 E, right). The average amplitude of the sPSCs was not significantly affected (P = 0.14; Fig. 5, D and E, left).

Collectively, these results indicate that the predominant input to NG2 glia is mediated by the AMPA subtype of ionotropic glutamate receptors.

NG2 glia and principal neurons receive common input

To directly compare AMPA receptor–mediated sPSCs in neurons and NG2 glia, we simultaneously recorded sPSCs from closely apposed neurons and NG2 glia in the presence of 4-AP and 2 μM strychnine, 10 μM gabazine, 50 μM D-APV, and 10 μM MK-801 (Fig. 6). To determine whether the two cells receive common input, we analyzed the time relation between postsynaptic events in neurons and NG2 glia. We expected to see synchronized sPSCs in the principal neuron and the NG2 glia if both are contacted by the same presynaptic terminal (Fig. 6, A and B). We therefore determined the time difference between the peak of a given event in the NG2 glia and the closest event in the neuron. Plotting these data as a histogram showed a peak of events around 0 ms with a scatter of less than ±2 ms (Fig. 6 E; see also Fig. S3 B). We also performed a cross-correlation analysis, where we shifted the two current traces against each other by increasing time steps (step size, 1 ms) and

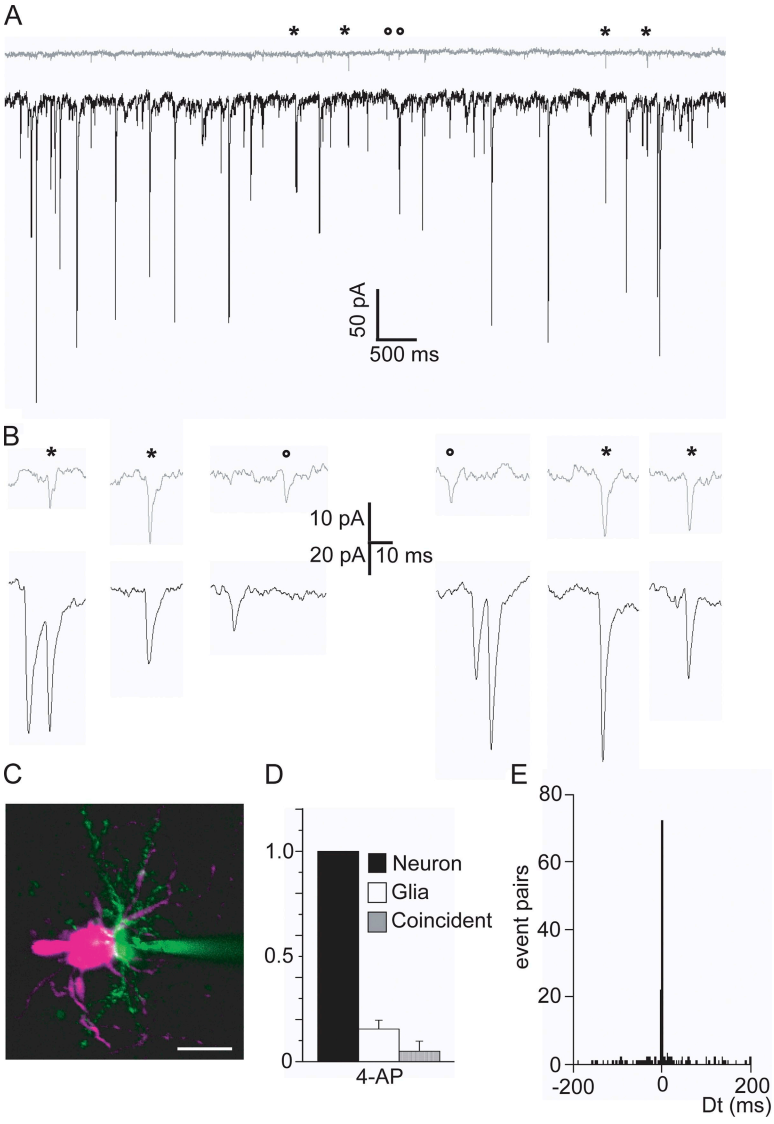

Figure 6. Coincident spontaneous synaptic activity recorded in NG2 glia and neurons. (A) Double whole cell recording showing the sPSCs in a principal neuron (black) and a closely apposed NG2 glia (gray) elicited by 100 μM 4-AP. The asterisks mark examples of coincident events, whereas the circles indicate examples of noncoincident events. Note the frequency difference in neuron and NG2 glia. (B) Representative sPSCs marked in A with higher time resolution. (C) Two-photon laser scanning microscope image of a recorded cell pair showing the neuron in magenta and the NG2 glia in green (filled with Alexa 594 and LY, respectively, through the patch pipette). Bar, 10 μm. (D) Summary of events in neurons, glial cells, and coincident events. The number of events was normalized to the number of events recorded in the neurons ($n = 9$). Data are the mean ± SD. (E) Time-difference histogram of events in glial cells related to neurons. The time difference between events in the two cells is plotted as a histogram with a bin width of 1.0 ms. Note the sharp peak around 0 ms.

Downloaded from http://rupress.org/jgp/article-pdf/134/2/115/1787105/jgp_200910194.pdf by guest on 05 December 2025

analyzed for coincidence. The amount of coincident events decreased abruptly to noise level when the traces where shifted by more than ±2 ms (Fig. S3 A), indicating that coincident events occur within a time frame of less than ±2 ms. Therefore, we considered only events within this time window as coincident. On average, 4.6 ± 4.6% (range of 0.7 to 13.3%) of the neuronal events and 32.1 ± 24.7% (range of 4.5 to 77.9%) of NG2 glia events were coincident (Fig. 6 D; $n = 9$). The average frequency of coincident events was 0.38 ± 0.60 Hz (range of 0.01 to 1.64 Hz; $n = 9$). The average frequency of noncoincident events in the NG2 glia was 0.41 ± 0.31 Hz (range of 0.16 to 1.15 Hz; $n = 9$), and 4.8 ± 3.5 Hz (range of 1.4 to 12.5 Hz; $n = 9$) in neurons. This indicates that NG2 glia and principal neurons in the MNTB share a significant part of their input.

Miniature postsynaptic currents

The amplitude histograms of the spontaneous events indicated a peak at 9–12 pA for NG2 glia and ~20 pA for neurons. To compare the quantal size in NG2 glia and neurons, we compared miniature spontaneous events (not depicted). We recorded membrane currents clamped at −70 mV in the presence of TTX and ruthenium red (Lim et al., 2003). To selectively record the excitatory events, we added 2 µM strychnine and 10 µM gabazine to the bath solution, thereby avoiding the reported increase in the amplitude of inhibitory sPSCs (Lim et al., 2003). In NG2 glia, the average single event was 12.56 ± 6.00 pA ($n = 106$ events; 7 cells). In neurons, the mean miniature excitatory postsynaptic current (mEPSC) amplitude was 16.51 ± 3.82 pA ($n = 270$ events; 6 cells). The decay time constant was similar for NG2 glia (1.64 ± 1.21 ms; 106 events; 7 cells) and neurons (1.85 ± 0.59 ms; 270 events; 6 cells; P = 0.67). The event frequency was 0.08 ± 0.06 Hz ($n = 7$) for NG2 glia and 0.19 ± 0.14 Hz ($n = 6$) for neurons. We observed no influence of ruthenium red on glutamatergic sPSC kinetics and amplitude, as reported by Trudeau et al. (1996).

Collectively, these results indicate that sPSCs and mPSCs in MNTB principal neurons as well as NG2 glia are comparable in amplitude.

DISCUSSION

The NG2 glia receives synaptic input

Our data indicate that the NG2 glia receives direct synaptic input from the CoH. Our ultrastructural analysis demonstrates that this input is possible because anatomically distinct axo-glial synaptic-like contacts are formed between processes of the NG2 glia and the CoH. Therefore, this unique type of glial cell represents a postsynaptic element that is integrated into the synaptic circuit of the MNTB. These findings support observations from other brain areas (Bergles et al., 2000; Lin and Bergles, 2004a,b; Jabs et al., 2005; Lin et al., 2005; Kukley et al., 2007; Ziskin et al., 2007) and further substantiate the concept that synapse-based information processing is a property not only of neurons, but also of certain types of glial cells. In the present study, we show that NG2 glia and MNTB principal neurons share common presynaptic input, or even, due to the architecture of the CoH synapse, probably from the same presynaptic terminal.

We found that two types of glial cells establish intimate contact with the CoH. One type is the classical astrocyte characterized by high levels of GFAP-eGFP expression, passive membrane properties, presence of glutamate transporters (not depicted), and extensive gap junction coupling. The other, termed NG2 glia in our study, is characterized by very low, if any, GFAP, but NG2 expression. In contrast to astrocytes, these cells are not coupled and have no glutamate transporters (not depicted), but they have glutamate receptors of the AMPA type. A similar cell type has been described in hippocampus, cerebellum, and corpus callosum (Bergles et al., 2000; Jabs et al., 2005; Lin et al., 2005; Ge et al., 2006; Ziskin et al., 2007). These cells are characterized by a voltage-dependent K^+ current profile with outward rectification, and this feature distinguishes them from the classical types of glial cells, namely astrocytes, microglia, or oligodendrocytes, both in gray or white matter (Berger et al., 1991; Matthias et al., 2003; Jabs et al., 2005).

NG2 glia receive glutamatergic input

The CoH is a giant glutamatergic terminal where evoked postsynaptic neuronal responses are mediated by a fast AMPA/KAR ($\tau < 3$ ms) or a slow NMDAR ($\tau > 50$ ms) EPSC (Forsythe and Barnes-Davies, 1993; Joshi and Wang, 2002). In our experiments, we placed the stimulation electrode at the midline, >300 µm away from the recording site, and used moderate stimulation intensities to avoid possible extracalyceal stimulation (Schneggenburger et al., 1999; Hamann et al., 2003). We observed large stimulus-induced currents in neurons as described previously (for review see von Gersdorff and Borst, 2002 and Schneggenburger and Forsythe, 2006). In the NG2 glia, we also recorded an evoked response with sensitivity to AMPA receptor antagonists and a decay time of <3 ms, but of smaller amplitude compared with the responses in the principal neurons. This indicates that electrically evoked responses in NG2 glia are mediated by AMPA/KAR, and that these inputs are most likely mediated by the CoH.

The glutamatergic response of the GluR cell in the hippocampus or the NG2 glia in corpus callosum and cerebellum also relies on AMPAR-mediated signaling (Jabs et al., 2005; Lin et al., 2005; Ziskin et al., 2007). In contrast to the hippocampus, where the GluR-type glial

Downloaded from http://rupress.org/jgp/article-pdf/134/2/115/1787105/jgp_200910194.pdf by guest on 05 December 2025

cells receive additional synaptic GABAergic input (Jabs et al., 2005), the NG2 glia in the MNTB showed mostly AMPA receptor–mediated spontaneous activity, with a remaining activity of <2% after blockade of AMPA/KAR. Therefore, we conclude that NG2 glia receive glutamatergic input through AMPAR, and that inhibitory input to NG2 glia is very low (if present at all) despite the cell's ability to respond to bath application of glycine and GABA (not depicted).

In contrast to its effect on NG2 glia, CNQX did not completely block the sPSCs in neurons, but this effect was only accomplished after blocking NMDA, glycine, and GABA receptors. In MNTB principal neurons, sPSCs mediated by glycine and GABA receptors were described previously (Lim et al., 2003). The pharmacological profiles of the AMPA responses in principal neurons and NG2 glia were similar to those reported for principal neurons in the rat MNTB (blocked by CNQX and with a decay time constant ≤3 ms) (Watano et al., 2004).

So far, we cannot unequivocally answer the question of the origin of the glutamatergic postsynaptic currents recorded from the MNTB NG2 glia. There are two types of glutamatergic terminals in the MNTB, namely the CoH and other non-calyceal terminals (Hamann et al., 2003). The stimulation protocol we used makes it quite unlikely to activate non-calyceal terminals when evoked responses are recorded (Schneggenburger et al., 1999). However, the situation is more complicated when spontaneous activity is recorded. Hamann et al. (2003) found a difference in kinetics between calyceal and non-calyceal events, with the calyceal ones being significantly faster than the non-calyceal ones. In our preparation, we found a significant difference in the glial versus neuronal rise time of the sPSCs recorded under control conditions. This difference can be due to differences in the spatial arrangement of the site where the response is initiated and where the recording electrode is placed. We assume that in glial cells, the event is initiated at the end of fine processes and thus a slowed response is recorded due to the length constant of the glial processes. However, when 4-AP was added, the rise time in the neurons increased significantly ($P < 0.001$), whereas no significant change could be observed in the NG2 glia ($P = 0.21$). A possible interpretation is that non-calyceal terminals are contacting the principal cell, but not the NG2 glia. Upon depolarization under 4-AP, the non-calyceal inputs are increasingly recruited and add to the increase in neuronal rise time. Because the increase was not observed in NG2 cells, we assume that they do not, or only to a negligible extent, receive non-calyceal contacts.

Possible mechanisms that promote 4-AP–evoked spontaneous currents

The enhancement of spontaneous events by 4-AP is sensitive to TTX in both neurons and NG2 glia, indicating that voltage-gated Na^+ channels and most likely action potentials are involved. However, an action potential spreading over the entire CoH elicits much larger currents in the neurons, as we observed and others have reported (for review see von Gersdorff and Borst, 2002; Schneggenburger & Forsythe, 2006). Ishikawa et al. (2003) reported that block of potassium channels by blockers such as TEA or 4-AP leads to an increase in the amplitude of EPSCs in the principal cells of the CoH due to a depolarization of the presynaptic terminal. They also found that 4-AP led to presynaptic action potential firing above 100 μM. Moreover, local depolarizing events, so-called spikelets, prepotentials, or d-spikes, have been reported in several brain regions (Stevens and Haas, 1996; Hughes et al., 2002; Crochet et al., 2004; Pinato and Midtgaard, 2005). However, at P8-P10, the CoH is not yet highly fenestrated (Kandler and Friauf, 1993; Ford et al., 2009), making a locally confined subthreshold action potential rather unlikely. Therefore, we interpret the amplitude increase as a 4-AP–induced small depolarizing event, leading to an increase in calyceal calcium concentration, which, in turn, results in a functional synchronization of a small number of release sites. In fact, Schneggenburger and Neher (2005) found that small and brief increases in presynaptic calcium can effectively change the release probability in the CoH.

We find it quite unlikely that the spontaneous currents are triggered by local increases of intracellular calcium, so-called calcium sparks (Llano et al., 2000). In dorsal root ganglion cells, 7–11 sparks are required to stimulate the release of one vesicle (Ouyang et al., 2005). This low efficiency of spark secretion coupling is in general agreement with findings in the CoH where ∼10 calcium channels control the release of a single vesicle (Meinrenken et al., 2002). Therefore, calcium sparks seem unlikely as an explanation for the observed postsynaptic currents with amplitudes of up to 300 pA that reflect synchronized release of ∼15 vesicles.

NG2 glia receive synchronized input together with the principal neuron

In our double recordings, about a third of the events in the NG2 glia were coincident with events in the neuron. The size and the kinetics of coincident events did not differ from noncoincident events. It is highly unlikely that the events in neuron and NG2 glia are coincident by chance (for the glial-neuron pair shown in Fig. 6; e.g., the probability is $2.9*10^{-98}$). We therefore can conclude that NG2 glia and MNTB neurons either share release sites or that release sites toward the neuron and NG2 glia are functionally coupled, forming groups that are synchronously activated. However, we cannot completely discard the possibility of non-calyceal excitatory inputs being responsible for the events recorded in MNTB NG2 glia.

Downloaded from http://rupress.org/jgp/article-pdf/134/2/115/1787105/jgp_200910194.pdf by guest on 05 December 2025

We find it most likely that the two thirds of noncoincident glial events are due to activity from a neighboring CoH. Indeed, NG2 glia are in contact with more than one CoH synapse based on our morphological inspection. Alternatively, the events could be from release sites that are exclusive to NG2 glia in combination with failures at the release sites toward the neuron. Although this assumption cannot be completely discarded, the high number of non-synchronized events in NG2 glia makes it unlikely.

The delay and amplitude of coincident events in NG2 glia

We found a consistent delay of the peak amplitude of ~0.5 ms in the coincident events recorded in NG2 glia as compared with the neuron (Fig. S3 B). The most likely explanation is a slower rise time of the current response due to the different spatial arrangement of the postsynaptic neuron and NG2 glia. The synapse at the neuronal site is axosomatic, and the recording electrode placed at the soma can record the time course of the event with little delay. The synaptic contact of NG2 glia is in most (if not all) cases between CoH and a process, and the recording electrode was placed at the soma of the glial cell. These processes are thin and long and, due to the length constant, the recording of the event is expected to occur with a delayed increase. This is indeed what we observed. This would also indicate that we underestimated the peak amplitudes of NG2 glial events. Although neurons had an mEPSC amplitude of 16 pA, it was lower in the NG2 glia, namely 12 pA. This difference could be partially due to this distant recording and/or explained by a lower release of glutamate at the glial synapse by a less efficient activation of the AMPA receptors due to a different type of ultrastructural arrangement, or by a lower number of receptors at the glial face of the membrane.

Synaptic input onto $NG2^+$ glial cells can regulate proliferation and development

The identification of synaptic signaling to NG2 glia opens the possibility that synaptic activity is involved in glial cell proliferation and differentiation. The cell fate of NG2 glia has received considerable attention but is not yet fully understood. The originally proposed name, $NG2^+$ oligodendrocyte precursor cell, stems from the fact that NG2 glia generate predominantly oligodendrocytes in the normal adult brain (Dawson et al., 2000; Horner et al., 2002). But it turned out that the environment is a crucial factor in determining NG2 glial fate because the cells have the capacity to be multipotent and can generate oligodendrocytes, astrocytes, and neurons (Horner et al., 2002; Belachew et al., 2003). From our study it is evident that NG2 glia in the MNTB receive glutamatergic synaptic input. Activation of glutamate receptors in $NG2^+$ oligodendrocyte progenitor cells is anti-proliferative (Gallo et al., 1996; Yuan et al., 1998). One could speculate that the glutamatergic input to NG2 glia serves to stabilize the population in an undifferentiated, non-proliferative state. In a pathological event, when this input is nonfunctional, the cells could proliferate and generate new cells.

We thank R. Jüttner for discussions and comments on the manuscript and for sharing chemicals, K. Karram and J. Trotter for providing antibodies, and R. Kröber for technical assistance.

This study was supported by a grant from the Deutsche Forschungsgemeinschaft (SPP 1172).

Edward N. Pugh Jr. served as editor.

Submitted: 12 January 2009
Accepted: 6 July 2009

REFERENCES

Barnes-Davies, M., and I.D. Forsythe. 1995. Pre- and postsynaptic glutamate receptors at a giant excitatory synapse in rat auditory brainstem slices. *J. Physiol.* 488:387–406.

Belachew, S., R. Chittajallu, A.A. Aguirre, X. Yuan, M. Kirby, S. Anderson, and V. Gallo. 2003. Postnatal NG2 proteoglycan-expressing progenitor cells are intrinsically multipotent and generate functional neurons. *J. Cell Biol.* 161:169–186.

Berger, T., J. Schnitzer, and H. Kettenmann. 1991. Developmental changes in the membrane current pattern, K+ buffer capacity, and morphology of glial cells in the corpus callosum slice. *J. Neurosci.* 11:3008–3024.

Bergles, D.E., and C.E. Jahr. 1997. Synaptic activation of glutamate transporters in hippocampal astrocytes. *Neuron.* 19:1297–1308.

Bergles, D.E., J.D. Roberts, P. Somogyi, and C.E. Jahr. 2000. Glutamatergic synapses on oligodendrocyte precursor cells in the hippocampus. *Nature.* 405:187–191.

Butt, A.M., J. Kiff, P. Hubbard, and M. Berry. 2002. Synantocytes: new functions for novel NG2 expressing glia. *J. Neurocytol.* 31:551–565.

Crochet, S., P. Fuentealba, I. Timofeev, and M. Steriade. 2004. Selective amplification of neocortical neuronal output by fast prepotentials in vivo. *Cereb. Cortex.* 14:1110–1121.

D'Ambrosio, R., J. Wenzel, P.A. Schwartzkroin, G.M. McKhann, and D. Janigro. 1998. Functional specialization and topographic segregation of hippocampal astrocytes. *J. Neurosci.* 18:4425–4438.

Dawson, M.R., J.M. Levine, and R. Reynolds. 2000. NG2-expressing cells in the central nervous system: are they oligodendroglial progenitors? *J. Neurosci. Res.* 61:471–479.

Elezgarai, I., A. Bilbao, J.M. Mateos, J.J. Azkue, R. Benitez, A. Osorio, J. Diez, N. Puente, F. Donate-Oliver, and P. Grandes. 2001. Group II metabotropic glutamate receptors are differentially expressed in the medial nucleus of the trapezoid body in the developing and adult rat. *Neuroscience.* 104:487–498.

Flores-Hernandez, J., E. Galarraga, J.C. Pineda, and J. Bargas. 1994. Patterns of excitatory and inhibitory synaptic transmission in the rat neostriatum as revealed by 4-AP. *J. Neurophysiol.* 72:2246–2256.

Ford, M.C., B. Grothe, and A. Klug. 2009. Fenestration of the calyx of Held occurs sequentially along the tonotopic axis, is influenced by afferent activity, and facilitates glutamate clearance. *J. Comp. Neurol.* 514:92–106.

Forsythe, I.D. 1994. Direct patch recording from identified presynaptic terminals mediating glutamatergic EPSCs in the rat CNS, in vitro. *J. Physiol.* 479:381–387.

Forsythe, I.D., and M. Barnes-Davies. 1993. The binaural auditory pathway: excitatory amino acid receptors mediate dual time-course excitatory postsynaptic currents in the rat medial nucleus of the trapezoid body. *Proc. Biol. Sci.* 251:151–157.

Downloaded from http://rupress.org/jgp/article-pdf/134/2/115/1787105/jgp_200910194.pdf by guest on 05 December 2025

Gallo, V., J.M. Zhou, C.J. McBain, P. Wright, P.L. Knutson, and R.C. Armstrong. 1996. Oligodendrocyte progenitor cell proliferation and lineage progression are regulated by glutamate receptor-mediated K+ channel block. *J. Neurosci.* 16:2659–2670.

Ge, W.P., X.J. Yang, Z. Zhang, H.K. Wang, W. Shen, Q.D. Deng, and S. Duan. 2006. Long-term potentiation of neuron-glia synapses mediated by Ca2+-permeable AMPA receptors. *Science.* 312:1533–1537.

Hamann, M., B. Billups, and I.D. Forsythe. 2003. Non-calyceal excitatory inputs mediate low fidelity synaptic transmission in rat auditory brainstem slices. *Eur. J. Neurosci.* 18:2899–2902.

Hamill, O.P., A. Marty, E. Neher, B. Sakmann, and F.J. Sigworth. 1981. Improved patch-clamp techniques for high-resolution current recording from cells and cell-free membrane patches. *Pflugers Arch.* 391:85–100.

Horner, P.J., M. Thallmair, and F.H. Gage. 2002. Defining the NG2-expressing cell of the adult CNS. *J. Neurocytol.* 31:469–480.

Hughes, S.W., K.L. Blethyn, D.W. Cope, and V. Crunelli. 2002. Properties and origin of spikelets in thalamocortical neurones in vitro. *Neuroscience.* 110:395–401.

Ishikawa, T., Y. Nakamura, N. Saitoh, W.B. Li, S. Iwasaki, and T. Takahashi. 2003. Distinct roles of Kv1 and Kv3 potassium channels at the calyx of Held presynaptic terminal. *J. Neurosci.* 23:10445–10453.

Jabs, R., T. Pivneva, K. Huttmann, A. Wyczynski, C. Nolte, H. Kettenmann, and C. Steinhäuser. 2005. Synaptic transmission onto hippocampal glial cells with hGFAP promoter activity. *J. Cell Sci.* 118:3791–3803.

Joshi, I., and L.Y. Wang. 2002. Developmental profiles of glutamate receptors and synaptic transmission at a single synapse in the mouse auditory brainstem. *J. Physiol.* 540:861–873.

Kandler, K., and E. Friauf. 1993. Pre- and postnatal development of efferent connections of the cochlear nucleus in the rat. *J. Comp. Neurol.* 328:161–184.

Kimura, M., N. Saitoh, and T. Takahashi. 2003. Adenosine A(1) receptor-mediated presynaptic inhibition at the calyx of Held of immature rats. *J. Physiol.* 553:415–426.

Kukley, M., E. Capetillo-Zarate, and D. Dietrich. 2007. Vesicular glutamate release from axons in white matter. *Nat. Neurosci.* 10:311–320.

Kuwabara, N., R.A. DiCaprio, and J.M. Zook. 1991. Afferents to the medial nucleus of the trapezoid body and their collateral projections. *J. Comp. Neurol.* 314:684–706.

Lim, R., S. Oleskevich, A.P. Few, R.N. Leao, and B. Walmsley. 2003. Glycinergic mIPSCs in mouse and rat brainstem auditory nuclei: modulation by ruthenium red and the role of calcium stores. *J. Physiol.* 546:691–699.

Lin, S.C., and D.E. Bergles. 2004a. Synaptic signaling between GABAergic interneurons and oligodendrocyte precursor cells in the hippocampus. *Nat. Neurosci.* 7:24–32.

Lin, S.C., and D.E. Bergles. 2004b. Synaptic signaling between neurons and glia. *Glia.* 47:290–298.

Lin, S.C., J.H. Huck, J.D. Roberts, W.B. Macklin, P. Somogyi, and D.E. Bergles. 2005. Climbing fiber innervation of NG2-expressing glia in the mammalian cerebellum. *Neuron.* 46:773–785.

Llano, I., J. Gonzalez, C. Caputo, F.A. Lai, L.M. Blayney, Y.P. Tan, and A. Marty. 2000. Presynaptic calcium stores underlie large-amplitude miniature IPSCs and spontaneous calcium transients. *Nat. Neurosci.* 3:1256–1265.

Mangin, J.M., A. Kunze, R. Chittajallu, and V. Gallo. 2008. Satellite NG2 progenitor cells share common glutamatergic inputs with associated interneurons in the mouse dentate gyrus. *J. Neurosci.* 28:7610–7623.

Matthias, K., F. Kirchhoff, G. Seifert, K. Huttmann, M. Matyash, H. Kettenmann, and C. Steinhäuser. 2003. Segregated expression of AMPA-type glutamate receptors and glutamate transporters defines distinct astrocyte populations in the mouse hippocampus. *J. Neurosci.* 23:1750–1758.

McAlpine, D. 2005. Creating a sense of auditory space. *J. Physiol.* 566:21–28.

Meinrenken, C.J., J.G. Borst, and B. Sakmann. 2002. Calcium secretion coupling at calyx of held governed by nonuniform channel-vesicle topography. *J. Neurosci.* 22:1648–1667.

Newman, E.A. 2005. Calcium increases in retinal glial cells evoked by light-induced neuronal activity. *J. Neurosci.* 25:5502–5510.

Nolte, C., M. Matyash, T. Pivneva, C.G. Schipke, C. Ohlemeyer, U.K. Hanisch, F. Kirchhoff, and H. Kettenmann. 2001. GFAP promoter-controlled EGFP-expressing transgenic mice: a tool to visualize astrocytes and astrogliosis in living brain tissue. *Glia.* 33:72–86.

Oliet, S.H., R. Piet, D.A. Poulain, and D.T. Theodosis. 2004. Glial modulation of synaptic transmission: insights from the supraoptic nucleus of the hypothalamus. *Glia.* 47:258–267.

Ouyang, K., H. Zheng, X. Qin, C. Zhang, D. Yang, X. Wang, C. Wu, Z. Zhou, and H. Cheng. 2005. Ca2+ sparks and secretion in dorsal root ganglion neurons. *Proc. Natl. Acad. Sci. USA.* 102:12259–12264.

Pinato, G., and J. Midtgaard. 2005. Dendritic sodium spikelets and low-threshold calcium spikes in turtle olfactory bulb granule cells. *J. Neurophysiol.* 93:1285–1294.

Renden, R., H. Taschenberger, N. Puente, D.A. Rusakov, R. Duvoisin, L.Y. Wang, K.P. Lehre, and H. von Gersdorff. 2005. Glutamate transporter studies reveal the pruning of metabotropic glutamate receptors and absence of AMPA receptor desensitization at mature calyx of held synapses. *J. Neurosci.* 25:8482–8497.

Sätzler, K., L.F. Sohl, J.H. Bollmann, J.G. Borst, M. Frotscher, B. Sakmann, and J.H. Lübke. 2002. Three-dimensional reconstruction of a calyx of Held and its postsynaptic principal neuron in the medial nucleus of the trapezoid body. *J. Neurosci.* 22:10567–10579.

Schneggenburger, R., and I.D. Forsythe. 2006. The calyx of Held. *Cell Tissue Res.* 326:311–337.

Schneggenburger, R., and E. Neher. 2005. Presynaptic calcium and control of vesicle fusion. *Curr. Opin. Neurobiol.* 15:266–274.

Schneggenburger, R., A.C. Meyer, and E. Neher. 1999. Released fraction and total size of a pool of immediately available transmitter quanta at a calyx synapse. *Neuron.* 23:399–409.

Stevens, D.R., and H.L. Haas. 1996. Calcium-dependent prepotentials contribute to spontaneous activity in rat tuberomammillary neurons. *J. Physiol.* 493:747–754.

Trudeau, L.E., R.T. Doyle, D.G. Emery, and P.G. Haydon. 1996. Calcium-independent activation of the secretory apparatus by ruthenium red in hippocampal neurons: a new tool to assess modulation of presynaptic function. *J. Neurosci.* 16:46–54.

von Gersdorff, H., and J.G. Borst. 2002. Short-term plasticity at the calyx of held. *Nat. Rev. Neurosci.* 3:53–64.

Watano, T., J.A. Calvert, C. Vial, I.D. Forsythe, and R.J. Evans. 2004. P2X receptor subtype-specific modulation of excitatory and inhibitory synaptic inputs in the rat brainstem. *J. Physiol.* 558:745–757.

Wu, S.H., and J.B. Kelly. 1993. Response of neurons in the lateral superior olive and medial nucleus of the trapezoid body to repetitive stimulation: intracellular and extracellular recordings from mouse brain slice. *Hear. Res.* 68:189–201.

Yuan, X., A.M. Eisen, C.J. McBain, and V. Gallo. 1998. A role for glutamate and its receptors in the regulation of oligodendrocyte development in cerebellar tissue slices. *Development.* 125:2901–2914.

Ziskin, J.L., A. Nishiyama, M. Rubio, M. Fukaya, and D.E. Bergles. 2007. Vesicular release of glutamate from unmyelinated axons in white matter. *Nat. Neurosci.* 10:321–330.

Downloaded from http://rupress.org/jgp/article-pdf/134/2/115/1787105/jgp_200910194.pdf by guest on 05 December 2025